Computational and Structural Biotechnology Journal 19 (2021) 3720–3734

COMPUTATIONAL AND STRUCTURAL BIOTECHNOLOGY JOURNAL

journal homepage: www.elsevier.com/locate/csbj

A hybrid stochastic/deterministic model of single photon response and light adaptation in mouse rods

Charlotte Johanna Beelen [a], Sabrina Asteriti [b,c], Lorenzo Cangiano [b,*], Karl-Wilhelm Koch [a], Daniele Dell'Orco [c,*]

[a] Department of Neuroscience, Division of Biochemistry, University of Oldenburg, 26111 Oldenburg, Germany
[b] Department of Translational Research, University of Pisa, Pisa 56123, Italy
[c] Department of Neurosciences, Biomedicine and Movement Sciences, Section of Biological Chemistry, University of Verona, 37134 Verona, Italy

ARTICLE INFO

Article history:
Received 4 April 2021
Received in revised form 19 June 2021
Accepted 21 June 2021
Available online 23 June 2021

Keywords:
Dynamic modeling
Phototransduction
Stochastic simulation
Light adaptation
Systems biology

ABSTRACT

The phototransduction cascade is paradigmatic for signaling pathways initiated by G protein-coupled receptors and is characterized by a fine regulation of photoreceptor sensitivity and electrical response to a broad range of light stimuli. Here, we present a biochemically comprehensive model of phototransduction in mouse rods based on a hybrid stochastic and deterministic mathematical framework, and a quantitatively accurate description of the rod impedance in the dark. The latter, combined with novel patch clamp recordings from rod outer segments, enables the interconversion of dim flash responses between photovoltage and photocurrent and thus direct comparison with the simulations. The model reproduces the salient features of the experimental photoresponses at very dim and bright stimuli, for both normal photoreceptors and those with genetically modified cascade components. Our modelling approach recapitulates a number of recent findings in vertebrate phototransduction. First, our results are in line with the recently established requirement of dimeric activation of PDE6 by transducin and further show that such conditions can be fulfilled at the expense of a significant excess of G protein activated by rhodopsin. Secondly, simulations suggest a crucial role of the recoverin-mediated Ca^{2+}-feedback on rhodopsin kinase in accelerating the shutoff, when light flashes are delivered in the presence of a light background. Finally, stochastic simulations suggest that transient complexes between dark rhodopsin and transducin formed prior to light stimulation increase the reproducibility of single photon responses. Current limitations of the model are likely associated with the yet unknown mechanisms governing the shutoff of the cascade.

1. Introduction

G protein-coupled receptor (GPCR) pathways mediate cellular signaling of diverse biological phenomena. Among those are the primary steps in vision taking place in vertebrate rod and cone photoreceptor cells. The rods' exquisite ability to respond to single photons has been the focus of intense decades-long research providing us with quantitative parameters of the main signaling steps involved: photoexcited rhodopsin (R) triggers activation of the G protein transducin (Gt) that interacts with a phosphodiesterase (PDE6), an enzyme with two very similar catalytic subunits, which in turn hydrolyzes cytoplasmic cyclic guanosine monophosphate (cGMP). Downstream targets of cGMP are cyclic nucleotide-gated (CNG) channels in the plasma membrane that close due to dissociation of cGMP, causing a decrease in an inward current and thus

Abbreviations: ADP, adenosine diphosphate; Arr, arrestin; ATP, adenosine-5′-triphosphate; BG, background illumination; cGMP, cyclic guanosine monophosphate; CNG, cyclic nucleotide-gated (channel); CSM, completely substituted mutant of rhodopsin; CV, coefficient of variation; DM, deterministic model; E, effector of the phototransduction cascade, activated PDE; FFT, fast Fourier-transform; G_α, α-subunit of the G protein; $G_{\beta\gamma}$, β- and γ-subunit of the G protein; GC, guanylate cyclase; GCAPs, guanylate cyclase-activating proteins; GDP, guanosine-5′-diphosphate; Gt, G protein/transducin; GTP, guanosine-5′-triphosphate; GPCR, G protein-coupled receptor; HSDM, hybrid stochastic/deterministic model; MPR, multiple photon response; PDE, phosphodiesterase 6; Ph, photons; R, rhodopsin; R_n, activated rhodopsin that has been phosphorylated n times; Rec, recoverin; RGS, regulator of G protein signaling; ROS, rod outer segment; RK, rhodopsin kinase; SD, standard deviation; SPR, single photon response; TTP, time to peak; ΔJ, photocurrent; ΔU, photovoltage.

* Corresponding authors.
E-mail addresses: lorenzo.cangiano@unipi.it (L. Cangiano), daniele.dellorco@univr.it (D. Dell'Orco).

https://doi.org/10.1016/j.csbj.2021.06.033
2001-0370/

membrane potential hyperpolarization [1]. As stated in numerous accounts, the precise operation of these visual cells needs sufficient amplification of the phototransduction pathway, followed by effective deactivation of all the activating steps, as well as feedback loops that adjust the cell to the daily changes in ambient light intensity [2]. For example, changes in Ca^{2+} concentration in the rod outer segment following the light activation of the cascade triggers negative feedback mechanisms on the guanylate cyclase (GC) by guanylate cyclase-activating proteins (GCAPs) and on the rhodopsin kinase (RK) by recoverin (Rec), both involved in the timely cascade shutoff [1].

High gain of receptor-G protein and receptor-effector coupling is considered a hallmark of phototransduction and GPCR signaling in general, but this assumption has been questioned in recent contributions. The number of activated effector PDE molecules was scaled down to as few as 12–14 per photoactivated rhodopsin in targeted experiments [3]. While the physiologically relevant numbers are still debated, other observations challenge the classical view of phototransduction. First, the GPCR rhodopsin is spatially ordered in track-like structures in the membrane of rod outer segment disks, and is thereby more restricted in its diffusion than previously thought [4–6]. Furthermore, in dark-adapted conditions, about 30% of transducin molecules might pre-assemble with rhodopsin [7,8], which could facilitate the light-triggered activation process in such a spatially ordered system [9–11], even though a contribution by Schöneberg et al. [12] questioned the significance of this phenomenon for efficient signaling, thus originating a debate on the physiological role of the pre-assembly [13,14]. Lastly, it has been recently proposed that the main effector in the cascade is not single-, but double-activated PDE [15], which would reduce the continuous noise in darkness by suppressing the spurious signal of spontaneous transducin activation [16].

A key role in dissecting the intricacies of this biochemical pathway is played by computer-assisted quantitative modeling of rod photoresponses, which has improved greatly in recent years based on the availability of robust experimental data. However, the role of dynamic pre-assembly of rhodopsin and transducin and the need for double-activated PDE described above have not been comprehensively addressed. Previous work demonstrates that modeling based on mass-action kinetics, while being an approximation for biochemical systems that better applies to well-stirred (i.e. homogeneous) volumes, may lead to accurate simulations of the photoresponse under different light regimes in amphibian [17–20], mouse [21,22] and zebrafish photoreceptors [23]. The mass-action approach has a few distinct advantages and a main disadvantage. The advantages are that it creates system-level complexity by virtually decomposing the signaling cascade into elementary steps, each described by parameters that have been either experimentally determined or estimated with relatively high confidence [24]. Moreover, simulations are quick, and the same model structure can be used to run both deterministic and stochastic simulations [25,26]. The disadvantage of this approach is that simulations are not space resolved and active species are not constrained to a small space, but are effectively 'diluted' over the entire reaction volume corresponding to the rod outer segment, where average concentrations are considered.

Here we present a hybrid stochastic/deterministic model that solves this conflict by scaling down the reaction volume in a comprehensive, system-level approach, that at the same time yields accurate results for the number of activated dimeric effector molecules [27] during the single photon response (SPR) and allows for fast simulations. Using this comprehensive phototransduction model we simulated individual SPRs in both wild type and mutant mouse rods, comparing them to both new and previously published electrophysiological recordings. Our model implementation allowed us to directly assess the effects of a lower gain of rhodopsin-PDE coupling as well as a dynamic pre-assembly of rhodopsin and transducin on SPRs. Finally, by extending the modelled conditions to light-adapting regimes, we were able to investigate the role of the Ca^{2+}-recoverin mediated feedback on rhodopsin kinase in light adaptation.

2. Materials and methods

2.1. Electrophysiology

Recordings were performed under approval by the ethical committee of the University of Pisa (prot. n. 2891/12) and conducted in accordance with Italian (D.lgs.vo 116/92) and EU regulations (Council Directive 86/609/EEC). Retinas from adult wild type C57Bl/6J mice were isolated as previously described [28]. Briefly, animals were dark-adapted for >2 h and anaesthetized by i.p. injection of urethane 20% W/V in 0.9% saline. Retinas were extracted under dim far red illumination through a corneal incision into cold bicarbonate-buffered Ames' medium (A1420; Sigma-Merck) and the vitreous removed. During all recordings, tissues were continuously superfused with Ames' equilibrated with 95%O_2/5%CO_2 and clamped at 37.0 °C using a custom-made controller [29] and a chamber holder capable of conditioning both liquid inflow and chamber base. The recording pipette tip solution contained (in mM) 90 potassium aspartate, 20 K_2SO_4, 15 KCl, 10 NaCl, 5 K_2PIPES buffer and was corrected to a pH of 7.20 with KOH/HCl. The recording pipette back solution had the same composition, with the addition of 0.4 mg/ml Amphotericin-B pre-dissolved in DMSO at 60 mg/ml for patch perforation. All recordings were made with an Axopatch 1D amplifier, low pass filtered at 1 kHz and acquired at 5 kHz with a Digidata 1320A and pClamp 9 software (Axon Instruments). Full field flashes and adapting backgrounds were delivered with a 520 nm LED, optionally conditioned by a 1.5 log units ND filter. Photon flux densities at the preparation were separately measured with a calibrated detector (1815-C/818-UV; Newport).

2.1.1. Patch clamp recordings of dim flash responses in dark adapted rods

Wholemount retinas were transferred, photoreceptor-side up, to the recording chamber. Perforated patch clamp recordings were obtained by sealing, under visual guidance and high magnification (IR illumination at 780 nm), directly onto rod outer segments using 15–30 MΩ fine pipettes. The seal was targeted to the outer half of the outer segment. Recordings were made in current clamp with the cell held at approximately −40 mV (i.e. near the photoreceptor unperturbed dark membrane potential V_{dark}) by manually adjusting the injected current. Liquid junction and Donnan potentials were not corrected for reasons discussed previously [28]. Consecutive dim flashes for SPR analysis (between 133 and 500 per rod) were delivered at ~2 s intervals. Flash strength was adjusted to obtain a balanced mix of failures, SPRs and multiple photon responses (MPRs). Time-to-peak (TTP) was measured on 11 Hz Gaussian lowpass-filtered records of the photovoltage to remove high frequency noise and avoid the phase delay introduced by our amplifier at high frequencies when operated in current clamp mode (Section 3.1). Gaussian filtering is symmetric and in our tests was found to significantly affect dim flash response TTPs only with cutoff frequencies well below 10 Hz.

2.1.2. Loose seal recordings of flash responses in dark- and light adapted rods

Retinas were cut into transverse slices of 250 μm thickness in cold Ames' as previously described [28] and transferred to the recording chamber. Loose seal recordings [30–32] were made in current clamp from rods located at some depth from the cut

surface in the outer nuclear layer. Flashes of increasing strength were delivered superimposed on different light backgrounds (Supplementary Fig. S1). Since this technique provides a scaled version of the rod photovoltage, for each background the average response was normalized between its baseline and maximal (i.e. saturating) response.

2.1.3. Patch clamp recordings of rod impedance

Perforated patch clamp recordings were made in a separate set of rods by sealing on the outer half of the outer segment with 14–16 MΩ pipettes. Membrane potential was held at −40 mV by constant current injection and sinusoidal current stimuli (50 s duration, T) were delivered while modulating their frequency between 0.1 Hz (f_{min}) and 30 Hz (f_{max}). These stimuli contained an equal representation in the time domain of each frequency decade (same time spent between 0.1 and 1 Hz as between 1 and 10 Hz) by varying frequency exponentially [33]:

$$f(t) = f_{max} 10^{\frac{(t-T)}{T} log(f_{max}/f_{min})} \quad (1)$$

The injected current waveform was thus:

$$i(t) = I_0 sin\left(2\pi \int_0^t f(t)dt\right) = I_0 sin\left(\frac{2\pi T f_{min}}{ln(f_{max}/f_{min})}\left(\left(\frac{f_{max}}{f_{min}}\right)^{\frac{t}{T}} - 1\right)\right) \quad (2)$$

Current I_0 was adjusted so as to obtain a small voltage response amplitude (a few mV peak-to-peak). For each rod, several sweeps were averaged and the complex input impedance obtained from the ratio of the voltage response fast Fourier-transform (FFT) to the current input FFT. The modulus and phase components of the complex impedance were extracted in the relevant range 0.1–30 Hz and averaged across recorded rods (n = 5).

In the same recordings we also delivered bright saturating flashes to assess the integrity of the phototransduction cascade when using somewhat larger pipettes to seal on the outer segment. In current clamp, the peak hyperpolarization had an amplitude of −27.1 mV (SD 2.7, n = 6) relative to the membrane potential just before the flash, while the subsequent plateau of −22.7 mV (SD 2.1, n = 6) (Fig. 1A_2) (the difference between the two is due to the bandpass impedance profile of rods). In voltage clamp, the peak photocurrent amplitude was 18.9 pA (SD 2.3, n = 5). These values are suggestive of a minimal disturbance to the phototransduction cascade.

3. Modeling

3.1. Rod impedance modeling and photovoltage to photocurrent conversion

First, we noted that the phase of the measured impedance crossed $-\pi/2$ at high frequencies (not shown). This should not occur with a cell behaving as an RC equivalent circuit, but could be due to the limited speed of our patch clamp amplifier when operating in current clamp mode via a high series resistance [34]. We inspected the theoretical frequency response of our system using a combination of different cell sizes and series resistances of up to 300 MΩ. While a small negative phase perturbation was indeed predicted to be introduced in the upper range of our explored frequencies, the impact on the amplitude was marginal under all conditions. We thus decided to fit the theoretical model described below only to the impedance amplitude.

We modelled the rod impedance at −40 mV by assuming that the inner segment expresses a time-dependent negative feedback conductance with a single time constant. In rods the two membrane conductances I_h (mediated by HCN1 channels; [35] and references therein) and I_{kx} (likely mediated by $K_v2.1$ channels; [36]) play such a role, each dominating in a particular range of physiological membrane potentials. The combined effect of these conductances and the passive properties of the cell membrane may confer a relatively constant band-pass behavior to rods over their entire physiological membrane potential range [35]. The rod inner segment impedance was modelled as [37]:

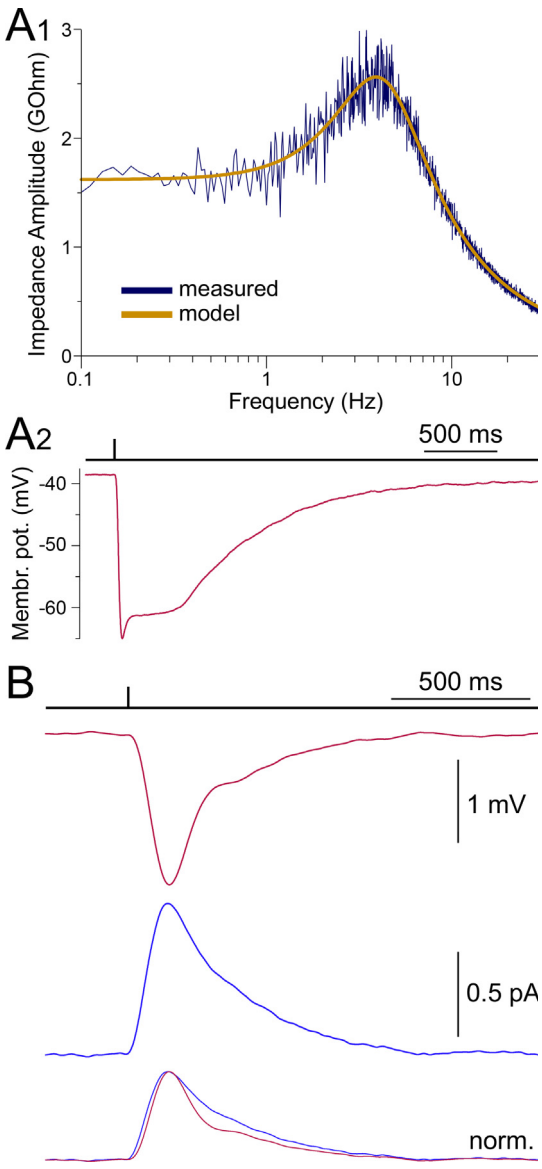

Fig. 1. The mouse rod impedance at −40 mV and its effect on dim flash responses. (A_1) The rod impedance amplitude at −40 mV and 37.0 °C obtained by patching on the outer segment (blue trace, average of 5 rods) is well reproduced by a model that assumes a negative feedback conductance with a single time constant in the inner segment and a resisto-capacitive outer segment (gold trace). (A_2) In the same outer segment recordings, bright flashes were also delivered to monitor the integrity of the phototransductive cascade; the trace shown is the average response of 6 rods. (B) Average recorded rod dim flash photovoltage response (upper trace) and after conversion to photocurrent using the impedance model (middle trace). The two are also shown normalized and superimposed (bottom trace). The photovoltage trace is the average from 9 rods, each contributing with the average of hundreds of individual responses (failures, SPRs and MPRs). Recordings were made in dark adapted rods by patching on the outer segment at 37 °C and holding the membrane potential near −40 mV by constant current injection (current clamp). Traces in panel B are 11 Hz Gaussian filtered. (For interpretation of the references to color in this figure legend, the reader is referred to the web version of this article.)

$$Z_{IS}(f) = \frac{1}{Y_{IS}(f)} = \frac{1}{g_{leak} + 2\pi i f c_{is} + g_{neg}[1 + H]} \quad (3)$$

where

$$H = \frac{\hat{g}}{1 + 2\pi i f \tau} \quad (4)$$

g_{leak} membrane passive leakage conductance
c_{is} membrance capacitance of the inner segment
g_{neg} negative feedback conductance, steady state value
$\hat{g}$ negative feedback conductance, deviation from ohmic behavior
τ negative feedback conductance, time constant

We connected the above inner segment compartment to a simplified outer segment compartment represented by a lumped membrane capacitance c_{os} (0.5 pF) and an internal axial resistance R_{os} (200 MΩ) [36]. The overall rod admittance as seen by a patch pipette sealed on the outer segment was thus described by:

$$Y(f) = \frac{1}{R_{os} + Z_{is}(f)} + 2\pi i f c_{os} \quad (5)$$

We fit this model to the average measured rod impedance amplitude, log-resampled to avoid overemphasizing high frequencies. This led to an excellent match (Fig. 1A_1) with the following set of parameters: g_{leak} = 97.373 pS, c_{is} = 13.624 pF, g_{neg} = 171.80 pS, $\hat{g}$ = 2.5358, τ = 64.434 ms. Recorded photovoltages were converted to photocurrents using the above model and parameters, by multiplying in the frequency domain the overall rod admittance Y(f) by the complex FFT of the photovoltage time series.

3.2. Categorization of the dim flash responses

To categorize the dim flash responses recorded with perforated patch clamp into failures, SPRs, and MPRs, we used the histogram method proposed by Hamer et al. [17]. To minimize the impact of noise on the categorization procedure, photovoltage records were low pass filtered with a running window filter (cut-off of ~11 Hz). Furthermore, slow drifts in membrane potential were removed. First, the average response was calculated (note that this is not the average SPR, but an average over all responses – including failures and MPRs). Next, each response was fitted to the rising phase of this average waveform, yielding a scaling factor. Such scaling factors were plotted as a histogram and three Gaussian distributions were fitted to the peaks, corresponding to failures, SPRs and MPRs. The intersections of the Gaussian distributions defined the limits of the scaling factors to categorize the responses into the above-named categories. This procedure is illustrated in Supplementary Fig. S2.

3.3. Kinetic models of phototransduction

The phototransduction cascade was simulated both under dim flash conditions, resulting in SPRs and MPRs, and under brighter light regimes by making use of two different kinetic models describing, respectively, a limited portion of the rod outer segment (ROS) and the whole cell compartment. Most of the biochemical reactions were described by a mass-action approach. Both of the models were created to match known experimental and modelling results, but not specifically to fit the novel experimental results presented here. The model of R* shutoff in both models is the following: Rhodopsin's affinity for transducin is exponentially decreased with each phosphorylation (up to 6 in the DM and up to 3 in the HSDM), while the affinity for Arrestin linearly increases – leading to a gradual shutoff as a function of the number of phosphorylations, and an abrupt shutoff upon binding to Arrestin.

In detail, the two models used in this work were the following:

- **Deterministic model (DM)**: A model describing the full ROS, used for bright light regimes. This model was simulated in a deterministic framework.
- **Hybrid Stochastic/Deterministic model (HSDM)**: A scaled-down model containing ~2 discs in a smaller volume, used for dim illumination. This model was simulated in a hybrid stochastic/deterministic framework.

In the deterministic model, there are hardly any double-activated PDEs because of the large volume: the activated transducin and single-activated PDE molecules are too diluted to create any double-activated PDEs. In contrast, in the hybrid stochastic/deterministic model, recent results concerning the dimeric nature of the effector and the number of effector molecules [3,15,16] were explicitly included. Due to the scaled-down nature of the model, we achieved a realistic amount of 12–14 double-activated PDE molecules during the single photon response. Further details about the two models are given below.

3.3.1. Building of the DM

The first model contains all relevant reactions for the phototransduction cascade according to a bottom-up network-level description [20,21]. Based on an extension of the model created in [21], the main change in the DM was a modification of the definition of effector towards a more realistic number, and a more detailed description of the regulation of guanylate cyclase activity by individual GCAPs, that is GCAP1 and GCAP2, as reported recently [38]. All known biochemical steps involved in the phototransduction cascade have been included in a bottom-up strategy. Supplementary Tables 1–6 list all the reactions and the relative kinetic parameters used in the numerical simulations.

Changes made to the original model by Invergo et al. [21] had very little effects on the response dynamics tested over a broad range of conditions. Comparisons between the outcomes of the two models are shown in Supplementary Fig. S3.

DM was used for deterministic simulations of the phototransduction cascade in bright and dim light conditions, when the average kinetics were of interest.

3.3.2. Building of the HSDM

PDE can be activated by up to two transducin molecules since it has two inhibitory and two distinct catalytic subunits [15]. Formerly, it was assumed that the single-activated PDE has half the maximal catalytic activity, while the double-activated PDE has the full activity. However, recent results [15,16,27] show that the single-activated PDE has a very low activity of less than 2.5% of the maximum. To account for this recent biochemical evidence, the main effector in our models was thus the dimeric G*PDE*G complex, and thus the effector was defined by:

$$E = 0.025\ PDE^{*} + PDE^{**} \quad (7)$$

where PDE^{*} and PDE^{**} represent single- and double-activated PDE, respectively.

In DM, indeed, the density of activated transducins is not high enough to create double activated PDE. Thus, the HSDM was implemented, which was scaled down to accommodate the new definition of the effector, whose main component is the double-activated PDE molecule. Due to the scaled-down volume, the relative concentration of activated species is higher than in the DM, which allows for the double activation of the PDE. Furthermore, the model was split in a stochastic frontend and deterministic

backend, which are illustrated in Figs. 2 and 3, hence defining a HSDM. The frontend model contains all the species influencing the effector: rhodopsin, rhodopsin kinase, arrestin, transducin and RGS. The backend model contains the second messengers cGMP and Ca^{2+} as well as the GC-GCAPs system, and uses the effector created by a simulation of the frontend model as an input. These molecular species do not require a stochastic simulation due to their abundance, but the stochastic nature of the response is already accounted for by the contribution of the effector. This split of the model is a trade-off between stochastic simulations of the relevant species and rapid simulations of the deterministic backend, which does not require stochastic treatment.

The HSDM was not suitable for bright light stimuli since only a small part of the ROS was simulated, and bright light stimuli could result in artefacts when the amount of free G protein available in the scaled down volume is depleted. Also worth noting, our analysis showed that the interaction of recoverin and the rhodopsin kinase was not relevant in the case of single photon or very dim light responses with no light background, and that rhodopsin molecules phosphorylated more than 3 times were so rare that they could be neglected (less than 0.01 rhodopsin with 3 phosphorylations at the peak of the single photon response in deterministic simulations, as can be seen in Supplementary Fig. S4). As a consequence, these species were either set to a constant value or omitted from the simulations.

When scaling down the HSDM model, the reaction rate parameters were scaled relatively to the DM corresponding to the change in volume, and some had to be further adapted. A full list of the parameters used in the simulations can be found in Supplementary Table 4.

3.3.3. Simulation and analysis of SPRs

To perform stochastic simulations of SPRs, two different types of initial conditions were used. In the first, the number of activated rhodopsin molecules per flash was fixed to one. This was ideal to compare the specific effects of different initial conditions on SPRs, such as those of dark R-Gt pre-assembly. The first type of initial conditions was not set randomly.

In the second, conditions were set to mimic those in actual rods, where one photon may be absorbed *on average* per flash, but each individual response may be a failure, SPR or a MPR. The number of absorbed photons was thus set randomly, described by Poisson statistics. We recreated this realistic scenario as follows:

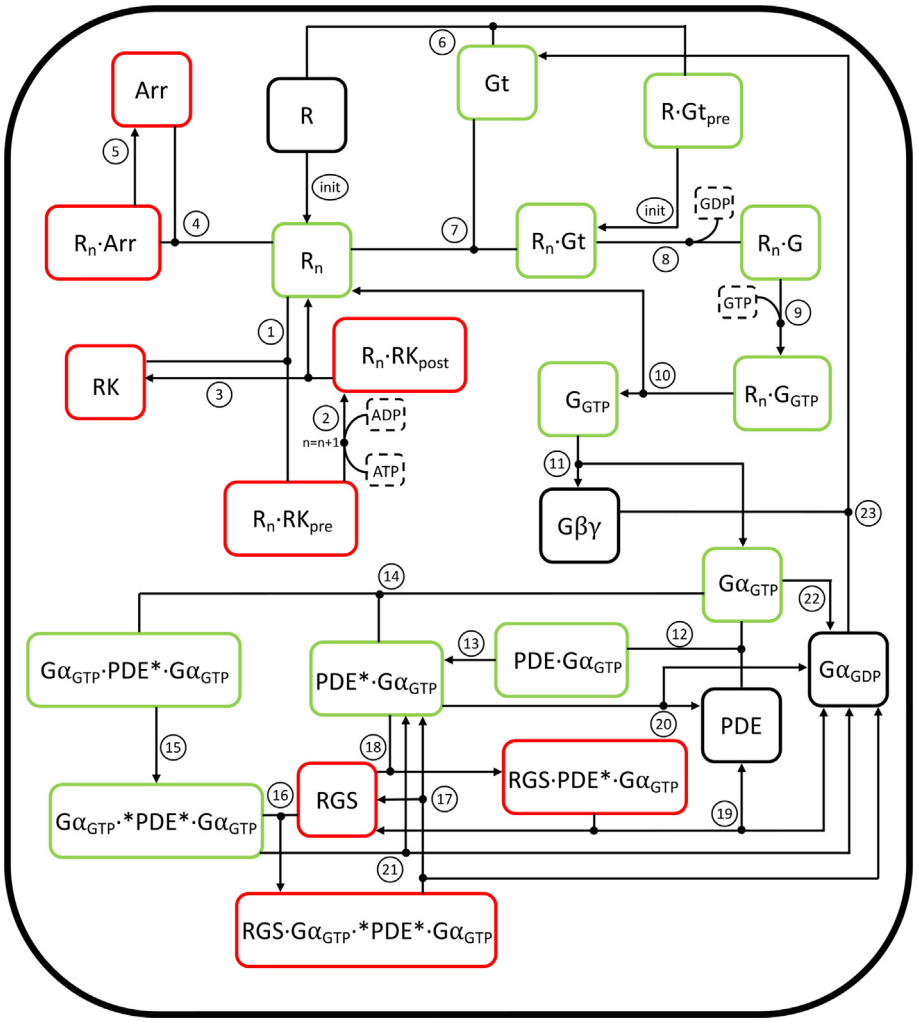

Fig. 2. Scheme of the reactions underlying the stochastic frontend of the HSDM. Molecular species are shown in boxes and reactions as arrows (irreversible) and connections (reversible). Reactions are numbered and listed in Supplementary Table 3. Species are color-coded according to their role in the cascade: species involved in the excitation phase are marked light green, while species involved in the shut-off of the cascade are marked red. R_n is rhodopsin that has been phosphorylated n times, and $R{\cdot}Gt_{pre}$ is a pre-assembled complex of inactive rhodopsin and G protein. The reactions marked "init" are the activation reactions, which are set as initial conditions in the HSDM. (For interpretation of the references to color in this figure legend, the reader is referred to the web version of this article.)

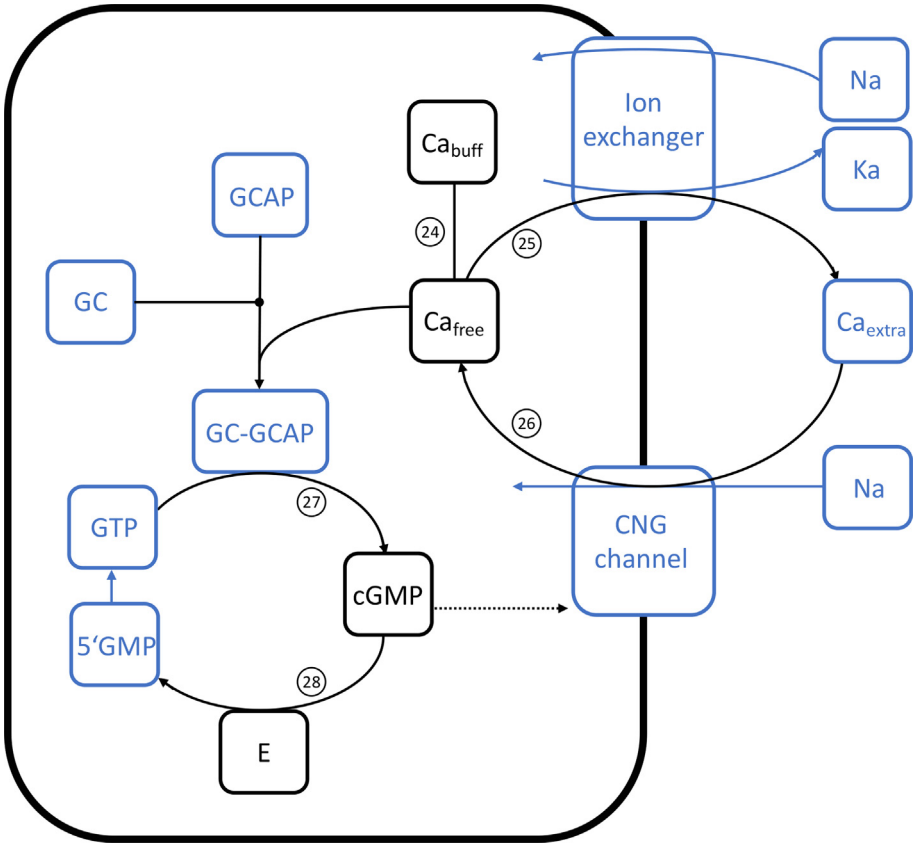

Fig. 3. Scheme of the deterministic backend of the HSDM. Molecular species are shown in boxes and reactions as arrows (irreversible) and connections (reversible). Species and reactions in blue are not contained explicitly, but implicitly in the model. Reactions are numbered and listed in Supplementary Table 6. The effector E is defined as E = PDE** + 0.025 PDE*. (For interpretation of the references to color in this figure legend, the reader is referred to the web version of this article.)

(i) a random Poisson number N was generated, representing the number of absorbed photons and thus activated rhodopsin molecules;
(ii) for each of these N rhodopsins it was determined whether they were pre-assembled to a G protein or not, proportionally to the probability of a random rhodopsin molecule being pre-assembled ([7]) (the amount of G protein being pre-assembled to dark rhodopsin was set to 18% of the total amount of G protein, which is a lower limit, like in [21]);
(iii) for each of the N activated rhodopsins, a separate stochastic simulation was run using a pre-assembled or non-pre-assembled rhodopsin as initial condition;
(iv) the simulation results were combined by summing over the separate traces for the effector, calculated as the weighted sum of PDE* and PDE**. Herein we assume that a multiple photon response consists of multiple simultaneous single photon responses that are taking place in the same rod, but sufficiently spatially separated to be independent.

The resulting stochastic traces for the effector were then used as input for the deterministic backend simulation, resulting in an ensemble of responses (failures, SPRs and MPRs), which could then be processed as and compared to the experimentally recorded dim light responses.

From the ensemble of responses, the subset of SPRs were analyzed using the coefficient of variation (CV) of the amplitude or the area, as done in previous quantitative accounts [17,18], defined as follows:

$$CV = \frac{\sigma}{\mu}$$

where σ is the standard deviation and μ the mean. As in other studies, when calculating the standard deviation σ, the variance of failures to respond was subtracted from that of the SPRs: $\sigma = \sqrt{\mathrm{Var}_{\mathrm{SPR}} - \mathrm{Var}_{\mathrm{fail}}}$.

3.3.4. Simulation of light adapted responses

Simulated responses with light backgrounds were generated by applying the same light stimuli in simulations as in the experiments, and scaling the experimentally-measured photon flux densities as follows: (*i*) all flashes and backgrounds were scaled by the same factor to account for variability introduced by water interface and tissue screening or refraction; (*ii*) the dimmest background was scaled separately due to photon flux density uncertainties occurring near the switch on threshold of the LED driver. Specifically, the scaling factor for the light intensities was 0.4, and the dimmest background was additionally scaled up by a factor of 3.

3.3.5. Model implementation and numerical simulations

Simulations were performed using MATLAB R2017b and the toolbox IQMtools V1.2.2.2 by IntiQuan (https://iqmtools.intiquan.com/). The stochastic simulations were run on the CARL cluster of the University of Oldenburg (Intel Xeon CPU E5-2650 v4 12C with 2.2 GHz) and the backend simulations on a desktop computer or laptop. Running a simulation of 100 SPRs took on the order of a few minutes.

All scripts used for running the simulations are available for academic use at: https://github.com/CBeelen/Phototransduction.

4. Results

4.1. Recordings of rod dim flash responses in dark adapted conditions

We obtained dim flash photovoltage responses in dark adapted rods at 37 °C with perforated patch clamp recordings made on the outer segments, using very small tip pipettes (Section 2.1.1). While the high access resistances associated with such combination ruled out using voltage clamp mode to acquire the photocurrent, we found that this approach greatly reduced a time-dependent run-down in kinetics prone to occur when recording from mouse rods [28,39]: the TTP of the dim flash response was essentially stable over a recording's useful duration (10–15 min from seal formation), with a rate of change of 0.46 ms/min (SD 2.83 ms/min; n = 8 rods). Flash strength was adjusted to obtain frequent failures.

The TTP of the average dim flash photovoltage response was 147.4 ms (SD 10.3 ms; n = 9 rods). We converted these traces from photovoltage to photocurrent using an experimentally-validated rod impedance model (Section 2.1.3 and Section 3.1, Fig. 1A_1). The TTP of the resulting responses was 142.9 ms (SD 14.3), only slightly lower than for the photovoltage although not yet significantly different with our sample size ($p = 0.07$; paired non parametric test). However, the width at 50% of response peak was much longer for the photocurrent at 273.5 ms (SD 56.0), compared to 180.0 ms (SD 28.6) for the photovoltage ($p < 0.01$) (Fig. 1B), reflecting the bandpass profile of the rod impedance.

For comparison to the simulations, filtered dim flash response photovoltages were categorized into failures, SPRs and MPRs by scaling each individual filtered trace to the mean response and separating them by their scaling factors (cf. Section 3.2 and Supplementary Fig. S2) (we used boxcar-filtered photovoltage data for the categorization). It must be noted that this procedure is notoriously challenging in mammalian rods and inherently affected by miscategorization errors (see below). For the two recordings where the categorization worked best, (i.e. best Gaussian fit results), the categorized responses were then converted to photocurrent. The ensemble failures, SPRs and MPRs with their respective averages can be seen in Fig. 4. We pooled the results from two recordings to arrive at a larger amount of responses compared to one recording. The coefficients of variation of the area and amplitude of the SPR were, respectively: $CV_{area} = 0.23$ and $CV_{amp} = 0.37$, while the TTP was 183 ms. The difference in TTP between the dim flash responses (see above) and the categorized SPRs was due to the fact that they were derived from non identical datasets and from the additional contribution of MPRs to the former population.

4.2. The HSDM reproduces well SPRs in mouse rods

Fig. 5 shows results from simulations of the HSDM. The initial condition was set to one activated rhodopsin molecule so that all 200 simulated responses were SPRs by design. Panel A shows the single photon traces and their average, as well as the result of simulating HSDM deterministically (which shows that the average stochastically simulated SPR corresponds to the deterministic result). Panel B shows the number of effector molecules as defined in Eq. (7), together with their average. The effector consists of typically 12–14 double-activated PDE molecules (PDE^{**}) as well as many (ca. 400) single-activated PDEs (PDE^{*}). The number of single- and double-activated PDEs contributing to the effector as well as the amount of activated transducin are shown in Supplementary Fig. S5.

When comparing the stochastic simulations to the experimentally recorded traces, two aspects are of relevance. The SPRs predicted by our model were slightly slower than the experimental ones: the TTP of the average experimental SPR was 0.183 s, while in our model it was 0.24 s. This slight delay was due to the specific modelling of the effector: the activation of each subunit of the PDE was split into two separate steps in the model, resulting in four reaction steps to full activation of both subunits. In tentative tests, we were able to identify that deleting the intermediate activation step reduced the time to peak and could potentially resolve this issue, but this would require further tuning of other parameters (Supplementary Fig. S6). While recent work cleared up the mechanism of transducin-PDE interaction [15,16], which leads to the formation of the effector, not all kinetic steps have been clarified; for instance, not much is known about the kinetics of the reactions that could introduce delay in the model (for instance, reactions #12 and #14, see Supplementary Table 3). When new experimental information will be available, this aspect could be further revised in future versions of the model.

Another moderate mismatch was found when comparing the coefficients of variation of the area and amplitude. These were: $CV_{area} = 0.23$ and $CV_{amp} = 0.37$ for the experiments, and $CV_{area} = 0.87$ and $CV_{amp} = 0.34$ for the simulations. Apparently, the dynamics leading to the amplitude of the SPRs were well reproduced in the model, but the area was not well reproduced. This may be due to

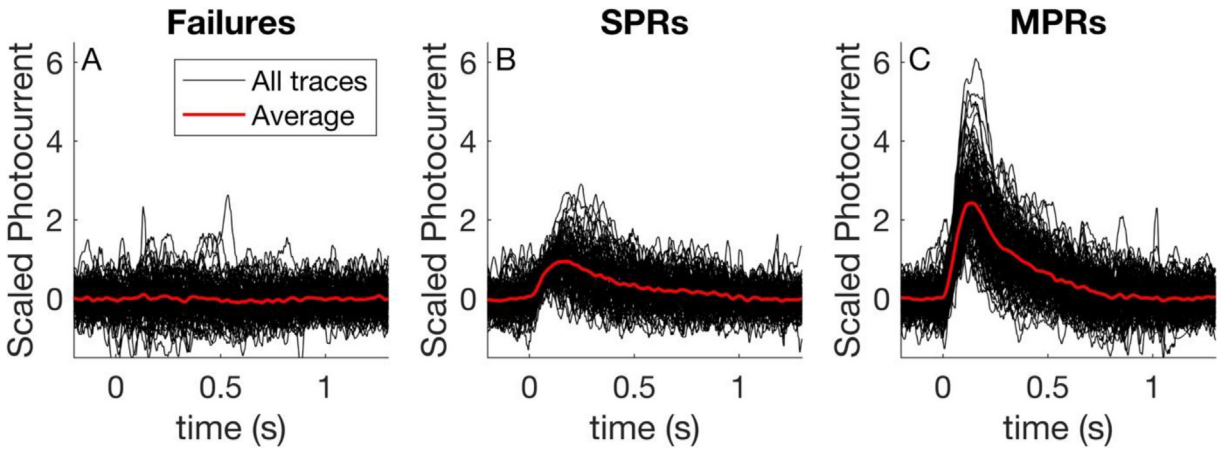

Fig. 4. Electrophysiological measurements (black) of dim flash responses (converted to photocurrent using the rod impedance model) categorized into (A) failures to respond, (B) SPRs, and (C) MPRs using the histogram method described in Section 3.2. The average of each set of traces is shown in red. The data are pooled from two separate recordings where the categorization procedure was most successful. (For interpretation of the references to color in this figure legend, the reader is referred to the web version of this article.)

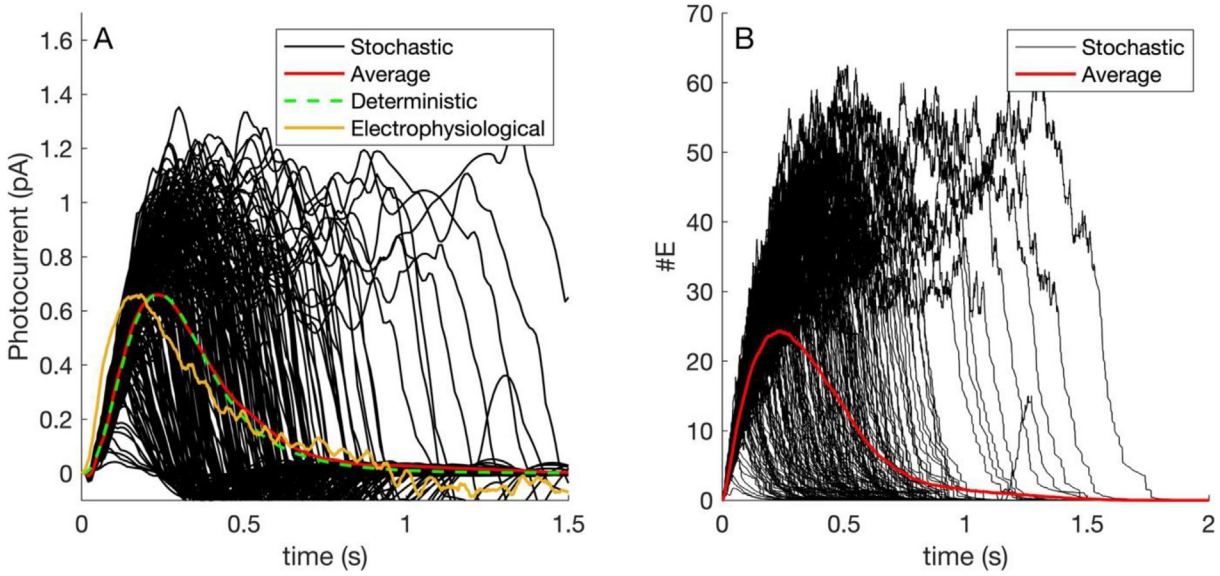

Fig. 5. (A) 200 stochastic simulations of SPRs (black) and their average (red) using HSDM, as well as the result of a deterministic simulation of HSDM (green) and the average electrophysiologically measured SPR (yellow). (B) The effector for the SPRs and its average. The effector is defined as follows: E = PDE** + 0.025 PDE* (Eq. (7)). (For interpretation of the references to color in this figure legend, the reader is referred to the web version of this article.)

the shutoff of the responses: longer SPRs may not be shut off strongly enough in the simulations, since the model might not accurately represent the relevant mechanisms (see Discussion). This may also be recognized in simulated SPRs with a prolonged plateau in Figs. 5A and 6B, which are not present in the experimentally recorded responses. The mismatch could also be due to the categorization process—see results on the stochastic simulations with random initial conditions (paragraph 4.3 and Fig. 6).

In spite of these caveats, the HSDM model quantitatively reproduced characteristic features of the phototransduction cascade during SPRs: 12–14 double-activated PDE** were observed at the peak, which combined with the activity of the single-activated PDE gives an effector number of about 25 (Fig. 5B). This is consistent with recent results concerning the number and nature of the main effector [3,15].

4.3. Simulations with random initial conditions

We also performed simulations with random initial conditions to mimic those occurring in actual rods, where dim flashes lead to a mixture of failures, SPRs and MPRs. In this extension of the model the number of activated rhodopsin molecules followed a Poisson distribution. Furthermore, each of the activated rhodopsins was either randomly pre-assembled to a G protein, or not, according to prior studies [7]. The random mixture of simulated responses was then categorized using the same procedure used for the experimental ones.

The results of the categorization of 200 such simulations are shown in Fig. 6. Interestingly, we could now actually compare the "true" SPRs to the categorized SPRs since we knew the initial conditions for each trace. When analyzing this, we noticed that five SPRs had been categorized as failures to respond, and five MPRs had been categorized as SPRs (these 'miscategorized' responses are shown in the Supplementary Fig. S7). This effect inevitably led to a systematic lower estimate of the variability of the categorized SPRs (CV_{area} = 0.86 and CV_{amp} = 0.29) compared to the 'true' ones (CV_{area} = 0.93 and CV_{amp} = 0.38).

4.4. Pre-assembly of dark rhodopsin with transducin decreases the variability of the SPR

We further tested the effect of a dynamic scaffolding of rhodopsin and transducin, postulated in previous *in silico* [8–10] and *in vitro* [5,7] studies, which has been integrated in recent

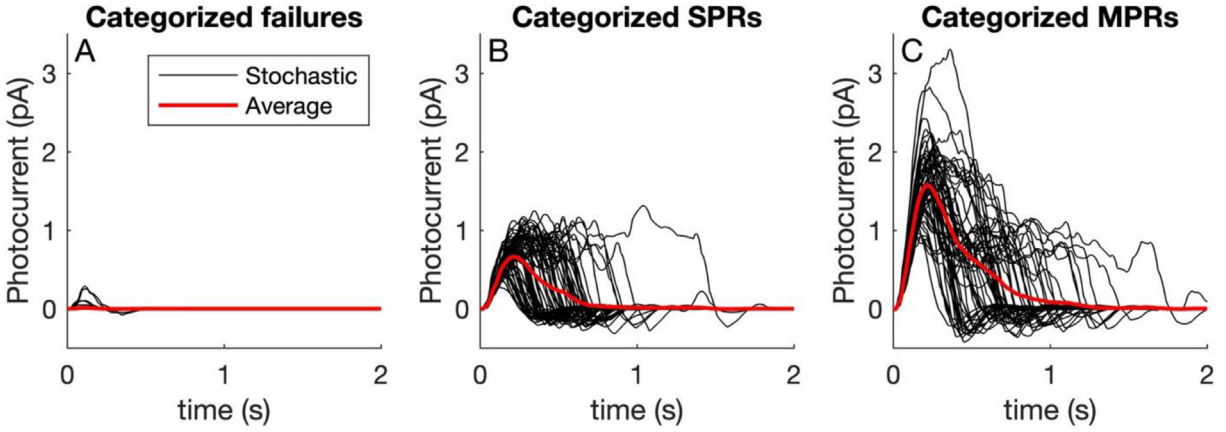

Fig. 6. Stochastic simulations of dim flash responses (HSDM) with random initial conditions, categorized into: (A) failures, (B) SPRs, and (C) MPRs, (200 in total), and their averages.

mechanistic descriptions of the phototransduction cascade [5,11]. Rhodopsin assembles into tracks of dimers in disk membranes thereby providing a platform for pre-assembling with transducin in the dark state [5]. This would allow transducin to interact rapidly with different rhodopsin molecules by either diffusing in the lipid milieu or hopping onto dark-adapted rhodopsin molecules following rapid association and dissociation [7,10]. It is unknown whether such a dynamic pre-assembly mechanism would affect the signaling cascade by any means, although previous modeling analyses performed in a deterministic framework suggested that the pre-assembly does not slow down the phototransduction cascade on a broad scale of dim to bright light stimuli [7]. We therefore tested the effect of the pre-assembly in the model and compared simulations of SPRs where the activated rhodopsin was pre-assembled to a G protein with simulations of SPRs where the activated rhodopsin was not pre-assembled. The effect of the pre-assembly in the stochastic simulations was quite small, but significant. There did not appear to be either a significant speed-up or slowing down of the SPR in the pre-assembled case (results not shown). However, the distributions of the areas and amplitudes resulting from the simulations appeared to be affected. Fig. 7 shows the distribution of areas and amplitudes resulting from a total of 1000 simulated SPRs for each initial condition – 1 activated rhodopsin, either pre-assembled or non-pre-assembled. For the pre-assembled case, the distribution appears sharper, and there are fewer responses with very low areas. The coefficients of variation of each distribution are reported in the corresponding subfigure.

There appears to be a slight decrease of the CV of the area (0.85 vs 0.90) and of the amplitude (0.34 vs. 0.36) of the distribution upon pre-assembly. This points to a slight reduction of variability of single photon responses due to the pre-assembly of dark rhodopsin and transducin.

4.5. HSDM recapitulates the salient features of photoresponses in genetically altered animals

An important aspect of the comprehensive modeling approach used here is its ability to reproduce, without parameter retuning, the rod photoresponses in mouse mutants with manipulated phototransduction genes. In particular, gene knockdown or overexpression pose severe kinetic constraints to models, and should be done without any parameter retuning in order to probe model robustness. Our implementation thus included only changes to the levels of expression of each modified gene, leaving all kinetic parameters unperturbed.

We compared the effect of several knockout mutations on SPRs recorded in prior studies: knockouts of rhodopsin kinase (RK) [40], of arrestin (Arr) [41], and of the GCAPs [42], as well as a completely substituted mutant (CSM) of rhodopsin which lacks all phosphorylation sites [43]. Experimental traces, with their respective wild type (WT) SPRs, are reproduced from previous studies in Fig. 8A, while the average SPRs resulting from 100 stochastic simulations are shown in Fig. 8B.

The knockout of both GCAPs (GCAP1 and GCAP2) leads to an impeded shutoff of the response. cGMP synthesis by the GCs is

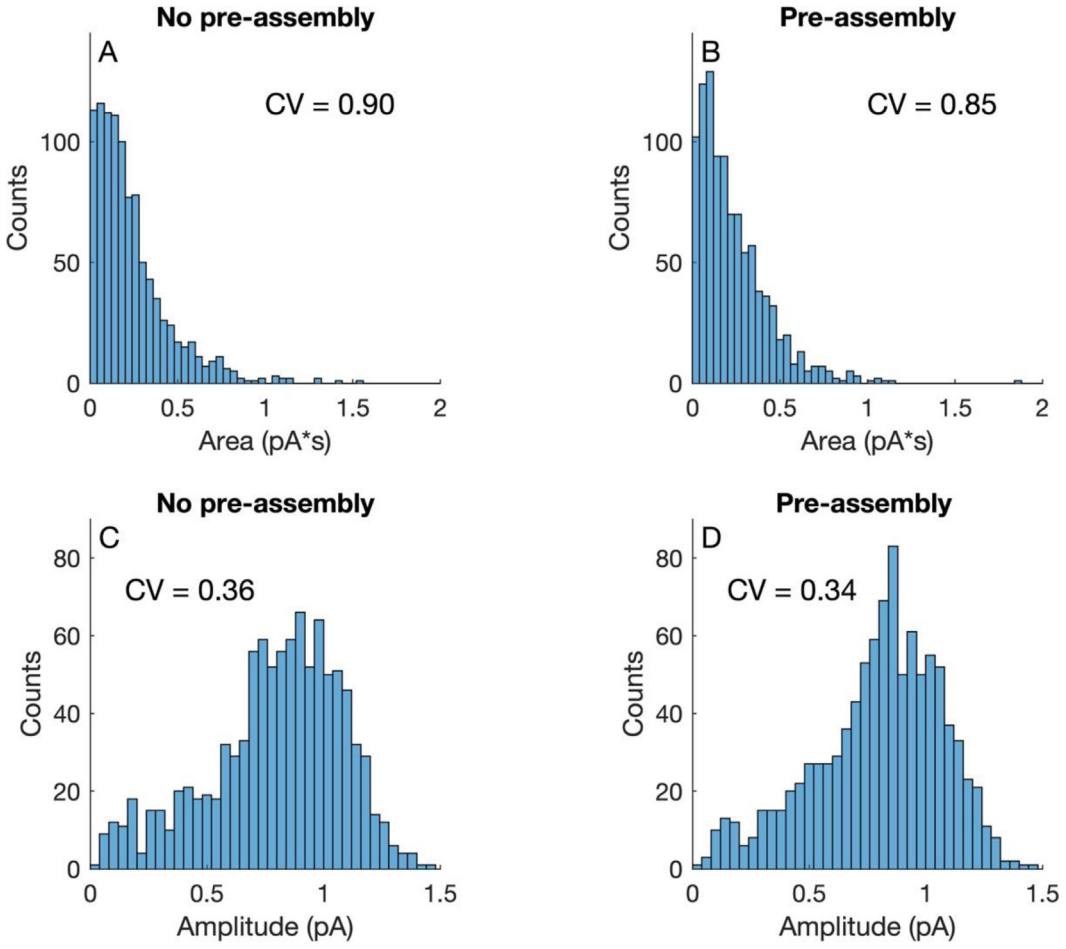

Fig. 7. The distributions of areas (A, B) and amplitudes (C, D) of 1000 simulated SPRs each for two different initial conditions: pre-assembled (B, D) and non-pre-assembled (A, C) activated rhodopsin. The corresponding coefficients of variation (CV) are provided in the panels.

not modulated by changes in intracellular calcium during the light response [44]. This leads to a higher average amplitude of the responses as well as a slower shutoff, due to the residual activity of the GC even without activation by the GCAPs. This behavior was well reproduced by our simulation.

The knockout of the rhodopsin kinase has the same effect as the expression of the rhodopsin mutant where all phosphorylation sites at its C-terminus have been disabled (CSM). Prevention of rhodopsin shutoff thus results in a larger amplitude of the SPR and very slow decay. The final shutoff can be achieved by the thermal decay of rhodopsin. This effect was qualitatively reproduced in our simulations.

The knockout of arrestin leads to an impeded decay of the SPR. Although rhodopsin can be phosphorylated, lack of arrestin prevents the complete stop of transducin activation. Here we noticed a difference between the simulated SPRs and the experimental ones: the simulated responses decay more slowly (see Discussion).

4.6. Recordings of rod flash responses in darkness and under light adapting backgrounds: comparison with DM simulations

We next extended our analysis by probing the performance of the DM under conditions of bright stimuli and light adaptation. For this purpose, flashes of varying intensities were delivered in dark-adapted conditions and in the presence of light-adapting backgrounds. In these experiments scaled rod photovoltages were recorded with the loose seal technique (Section 2.1.2), which offers extremely stable response kinetics even during long recordings (i.e. in excess of one hour) [30,31,39]. Five flashes, from dim to saturating, were delivered in order of increasing strength with enough time between flashes for recovery. This sequence was repeated for each of four increasing background intensities. Several sweeps were averaged together for each background. A series of recordings from a rod is shown in Fig. 9A. The corresponding stimulus protocol can be found in the Supplementary Fig. S1.

The TTP of the dimmest flash response in darkness was 137.8 ms (SD 9.4 ms, n = 5 rods), close to that observed in patch recordings from the outer segment (Section 4.1). We simulated responses to the same stimulation protocol using the DM. The light intensity had to be scaled for the simulations to take into account different sources of experimental variability and uncertainty (Section 3.3.4). In Fig. 9B-E, we compare the experimental responses to the first two (i.e. dimmest) flashes, converted to photocurrent, with the simulations. In the latter, the baselines and amplitudes were normalized to the experimental ones (each simulated response to its corresponding experimental response). The activation and recovery phases of the simulated responses were, similarly to what observed with the SPRs (Section 4.3), slower compared to the experimental results. This slight mismatch of simulation and experiment became more apparent for brighter flashes (not shown).

However, when we compared the effect of the background on reducing the time spent above half the maximal intensity for each flash (T_{half}), we observed that the simulations reproduced the general trend of the experimental results well. This can be seen in Supplementary Fig. S8, which reports on the reduction of T_{half} in experimental (left) and simulated (right) results.

4.7. Recoverin-mediated Ca^{2+} feedback on rhodopsin kinase is a necessary mechanism for light adaptation

The regulation of rhodopsin phosphorylation by a Ca^{2+}-feedback on rhodopsin kinase is crucial for shutting off the phototransduction cascade. The feedback is operated by recoverin that, in its myristoylated form, can switch between functionally distinct states in the presence of disc membrane and rhodopsin kinase [45]. We investigated the effect of removing this feedback mechanism in the DM, and deleted the mechanism when splitting the model into a stochastic frontend and a deterministic backend for the stochastic simulations.

For flashes on dark-adapted rods, there was no effect from the removal of the Ca^{2+}-mediated feedback as shown in Supplementary Fig. S9 (left). However, when simulating rods adapted to a light background, the recovery time to the dark state after a bright flash was impacted by the removal of the feedback. This can be seen in Fig. 10 – specifically, in the full model (Fig. 10A), adaptation to backgrounds of different intensities led to a speedup of the recovery that was more pronounced the brighter the background intensity, in line with the paradigm of light adaptation [19]. When the Ca^{2+} feedback via recoverin and the rhodopsin kinase was removed, this light adaptation effect vanished: regardless of the background intensity, the recovery took the same time, which

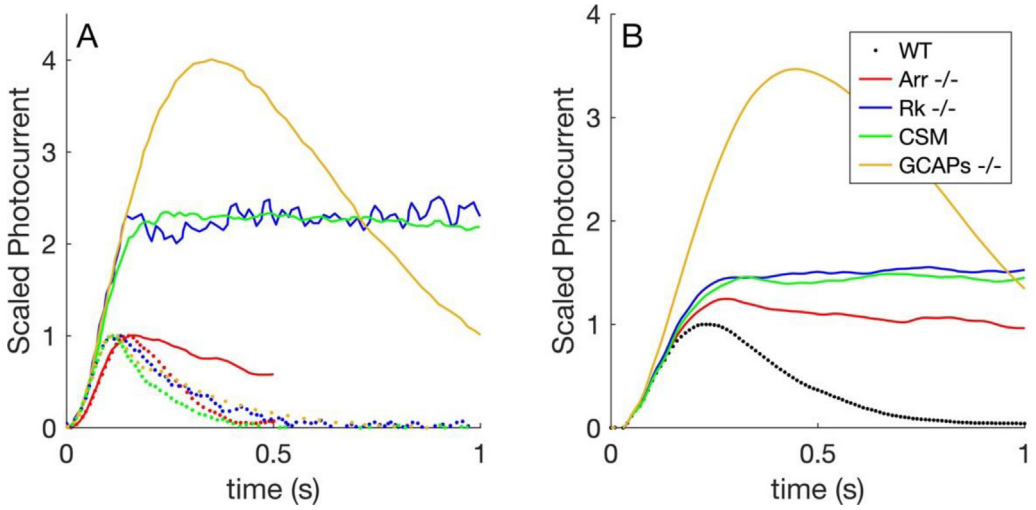

Fig. 8. (A) Experimentally measured SPRs, and (B) simulated SPRs, in the following conditions: Arrestin knockout (red, from [41]), rhodopsin kinase knockout (blue, from [40]), completely substituted mutant (green, from [43]) and GCAPs knockout (yellow, from [42]). The responses have been scaled so that their respective WT responses have a SPR amplitude of 1. The simulated results are averaged from 100 simulated SPRs each. The corresponding wild type responses are plotted in dotted lines in the respective colors in the left plot and in a dotted black line in the right plot. (For interpretation of the references to color in this figure legend, the reader is referred to the web version of this article.)

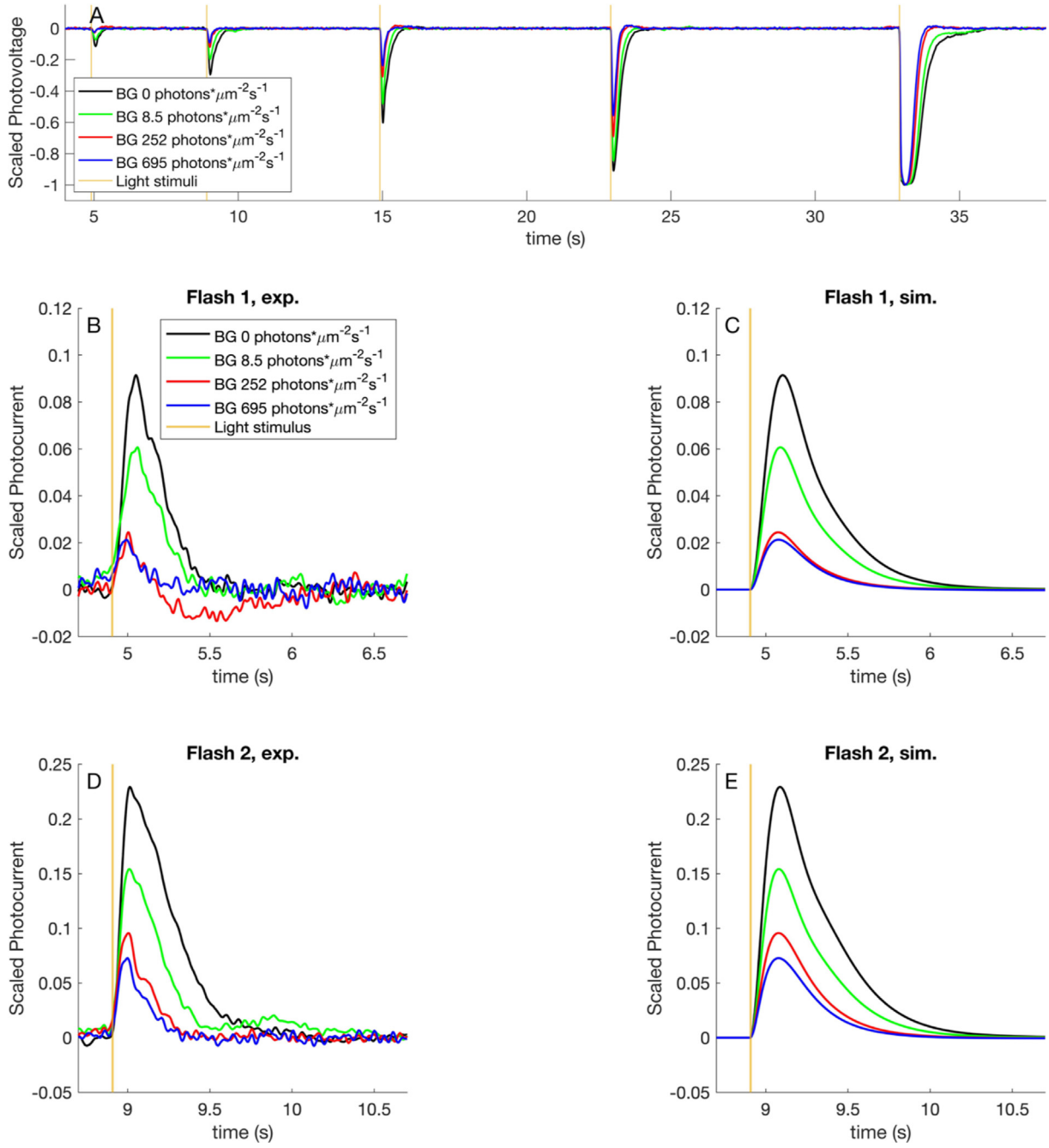

Fig. 9. (A) Loose seal rod photovoltage recordings at body temperature showing responses to 5 flashes of increasing strength (from 9.5 to 5,104 photon/μm^2, see Fig S1) in the presence of 4 different light backgrounds. This technique ensures unperturbed response kinetics but requires separate normalization for each background between baseline and saturation (brightest flash peak response). Records are averages of several sweeps. (B-E) Comparison of the experimentally recorded (left) and simulated (right) flashes 1 and 2 (9.5 and 32.1 photon/μm^2), the two dimmest flashes. The simulated responses have been baselined to a resting current of zero to match the experimental recordings, and normalized to the same peak amplitudes as the experimental traces for each trace. The experimentally recorded photovoltages have been converted to photocurrents. The timing of the stimuli is indicated by vertical yellow lines. (For interpretation of the references to color in this figure legend, the reader is referred to the web version of this article.)

can be seen in Fig. 10B. Supplementary Fig. S9 (right panel) shows the saturation time over the logarithm of the light intensity, where the same effect can be observed. This behavior was partly predicted in the model developed by Hamer et al. [18] although the more detailed representation of the recoverin (Rec)-mediated calcium feedback on rhodopsin kinases implemented by Invergo et al. [20] and re-proposed in our model probably leads to a better recapitulation of the acceleration of the bright flash response recovery following background light.

5. Discussion

Rod phototransduction offers the unique possibility to simulate experimental physiological responses triggered by light with computationally assisted mathematical modelling. So far, no GPCR signaling system other than the phototransduction cascade offers robust physico-chemical parameters derived from experiments that can be integrated into mathematical models for direct comparison with experimental data. An advantage of the

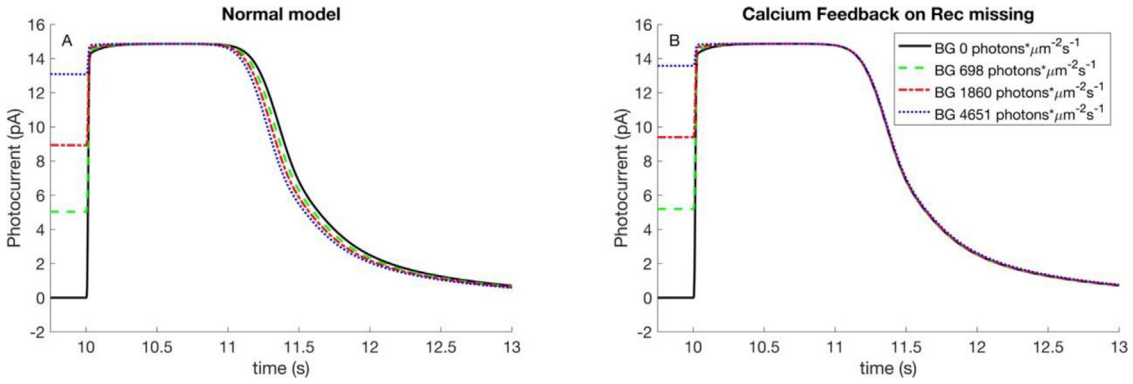

Fig. 10. Simulated responses of models adapted to different backgrounds for 10 s, after which follows a saturating flash. In (A), the calcium feedback on recoverin and the rhodopsin kinase was included in the model, while in (B) it was left out.

phototransduction modelling presented here is that its modular bottom-up structure permits to ask specific questions based on recent findings that had not been addressed in previous computational investigations. We present a novel modeling framework, in which a comprehensive model that has shown the capability to reproduce experimental responses in amphibian [19,20] and mouse [21] photoreceptors, has been modified to account for novel experimental mechanisms regulating the phototransduction cascade. With minor parameter tuning, the model has been scaled down to allow both the simulation of responses generated by very dim light sources, which required a stochastic implementation (HSDM), and responses to brighter light conditions including the adaptation to different backgrounds of light, in a deterministic framework (DM).

SPRs were recorded from mouse rods at 37 °C and a comparison with our simulated photoresponse using the HSDM showed overall good consistency, in spite of the choice of not tuning model parameters to obtain a better match. This indicates that the structural modifications to the DM, mostly at the effector side, and the scale-down process were necessary steps for obtaining realistic results by overcoming the well-stirred approximation, unsuitable for the few molecular events occurring on individual discs. The hybrid nature of our modeling allowed us to test recent findings about the G protein-effector gain and the impact of the dimeric activation of the phosphodiesterase PDE by the G protein transducin [15]. By combining single-activated PDE with double-activated PDE, the number of activated effector molecules (given by the weighted sum of PDE* and PDE**) was reduced from ca. 100 to around 25, when the modelled SPR reaches its peak (Fig. 5). These numbers are in agreement with a recent modelling approach by Lamb et al. [16,27] who also took into account the dimeric activation of the PDE by transducin. Those modeling studies concluded that the dimeric nature of PDE activation may decouple it from the spontaneous activation of transducin, thus resulting in a reduction of the continuous dark noise in rods [16]. The result was an improved quantitative model of phototransduction based on three combined approaches: (*i*) simulation of the bidimensional diffusional molecular interactions at the disc surface; (*ii*) a faster mass-action kinetics implementation assuming spatial homogeneity on the disc membrane; (*iii*) a model based on (ii), which additionally accounted for aberrant shutoff of photoactivated rhodopsin molecules in different discs [27]. The simulated photoresponses based on this effective mix of space resolved, stochastic and deterministic modeling qualitatively matched well the shape of mammalian bright-flash responses in rods [27]. However, while being an accurate tool, the essentially reductionist modeling framework used in that work does not allow the comprehensive analysis of all other components of the phototransduction cascade considered here, whose complex interplay poses severe kinetic constraints to the photoresponse shape and dynamics, both at dim and bright light conditions [19]. Furthermore, due to the nature of the space resolved simulations, these simulations are quite time-consuming, while our hybrid scaled-down model allows for rapid execution of simulations (within the order of minutes).

The hybrid scaled-down model could also help in interpreting the object of a current dispute on the gain of the phototransduction cascade in conditions corresponding to the SPR. Yue et al. [3] recently claimed that the effective gain expressed as the number of effector molecules, that is the complex between activated PDE and transducin, can be as low as 12–14 per active rhodopsin, being therefore significantly lower than previous determinations obtained from apparently less intact cell preparations. Our simulations match the determinations by Yue et al. [3] when the effector is considered as the weighted sum of single and double activated PDE bound to the G protein (Fig. 5 and Supplementary Fig. S5), however they also show that, in order to achieve approximately 25 activated effector complexes in an average SPR, which means 50 activated transducins, many more activated (~450) G proteins per activated rhodopsin are needed. Heck et al. [46] pointed out that the actual number of activated transducin per SPR can add up to 40–50, which is based on the observation that (*i*) full activation of PDE needs two transducin molecules; (*ii*) a fraction of transducin is single bound to PDE and thus almost ineffective in PDE activation; (*iii*) a fraction of G proteins is unbound or has become again inactive [46]. This would sum up to several hundreds of transducin molecules activated per second, but yields less than 100 considering an average lifetime of light-activated rhodopsin of 40–80 ms in agreement with our simulations (Fig. 5 and Supplementary Fig. S5). Hence, our results may reconciliate the two views in apparent contradiction [3,46]. The requirement of double activation of PDE (implying a 2:1 G:PDE effective stoichiometry) may be fulfilled at the expense of a significant excess of G proteins activated by rhodopsin, which could either bind to PDE forming inefficient single PDE* complexes or spontaneously deactivate, thus not meant to carry on the amplification cascade. The latter possibility has been discussed by some of us earlier [9] in an attempt to assess a possible role of the supramolecular organization of rhodopsin and transducin in setting the phototransduction kinetics.

We further tested the influence of a preformed complex between dark rhodopsin and transducin at the disk membrane on the kinetics and shape of the photoresponse. Computational analyses of the molecular structure of dark-adapted rhodopsin and GDP-bound transducin suggested that the two proteins may form a transient complex prior to photon absorption by rhodopsin [8,47,48]. Experimental evidence for a transient pre-assembled complex was indeed collected *in vitro* and a fraction of transducin

molecules (approximately 25%) in the outer segment were estimated to be pre-coupled to dark-rhodopsin [7]. It should however be noted that this value constitutes a lower limit, whose estimate is strongly influenced by the concentration of rhodopsin and transducin in the whole outer segment. The experimentally determined equilibrium constants are indeed consistent with up to 90% of G proteins being dynamically pre-assembled with rhodopsin in the dark and rapidly dissociating [7], therefore the actual situation at the level of individual discs could lead to a higher number of pre-assembled dynamic complexes. If a fraction of transducin is pre-coupled to rhodopsin in the dark, one could intuitively assume that such a complex would immediately become active without an intermediate diffusion step causing to speed up the response. Previous simulations suggested that the dynamic pre-assembly would not perturb the kinetics of photoresponses, although the analysis did not consider spatial constraints and was not performed in a stochastic framework [7]. The kinetics of this process in the context of the identified supramolecular organization of rhodopsin in tracks of dimers has been recently investigated [5,11]. In the present simulations, we did not observe any change in the kinetics of the photoresponse, neither an acceleration nor a slowing down, when we incorporated parameters describing the pre-assembled state in the model. However, the distributions of the areas and amplitudes of the single photon responses turned out to be different compared between the pre-assembled and non-pre-assembled case, and point to a lower variability in the presence of pre-assemblies. It should be noted that the results of our simulations are independent of the fraction of rhodopsin that is pre-assembled to transducin, since we directly compared the pre-assembled and non-pre-assembled initial conditions. Our results thus indicate that the illumination of rhodopsin in pre-assembled complexes leads to responses with less variable areas and amplitudes. At present, we have no proof for this assumption, but one could speculate that keeping a significant fraction of transducin less mobile (or transiently fixed to its upstream binding partner according to the dynamic scaffolding hypothesis) would decrease any failing rate that might occur. Larger and less variable areas and amplitudes could be beneficial for the transmission of SPRs in retinal neurons [49,50].

Beside the generally good performance of our stochastic simulations in comparison with experimental records in terms of overall dynamics and statistics, some specific caveats have to be considered carefully. First, our analysis of stochastically simulated SPRs with randomized initial conditions showed that the method of categorizing dim light responses into failures, SPRs and MPRs can lead to an underestimation of the CV. This systematic (albeit unavoidable) error was recently suggested by Lamb et al. [16] to contribute to the markedly smaller amplitude and area CVs of SPR estimated from rod recordings compared to those obtained in simulations. Our present findings quantitatively support this interpretation and imply that miscategorization of electrophysiological data gives an inaccurate representation of the underlying variability in rod SPRs. Furthermore, they serve to highlight how numerical simulations effectively extend our experimental tools beyond *in vitro* and *ex vivo* approaches.

A slight discrepancy was observed also when simulating SPRs from mice with genetically altered photoreceptors (Fig. 8). Although the agreement between experimental and simulated photoresponses was generally good, simulation of arrestin knockout rods led to slower recovery compared to experimental curves. This could be due to several factors. First, the model only contains one species of arrestin, which completely fulfills the purpose of shutting off rhodopsin, while native rods have two types of arrestin [51]. The second form of arrestin, named p44, is not knocked out in the experimentally recorded trace and could compensate partially the lack of the other isoform. Second, modelling the shutoff effect based on phosphorylation and subsequent arrestin binding might lack critical parameters and/or mechanisms that had not been identified so far. This model indeed is based on an extension of a previous comprehensive model [21] that was especially sensitive to the affinity of rhodopsin kinase for phosphorylated rhodopsin. Further experimental evidence, which is currently lacking, is needed to refine this mechanism thereby improving the match with experimental recordings. This missing mechanism could as well partly explain the discrepancy observed between experimental and simulated CV values for the area and the amplitude of SPRs, as well as the SPRs with a prolonged shutoff that we only observe in the simulated responses.

Another achievement of this study is the extraction of a quantitatively accurate descriptive model of the mouse rod impedance in darkness, which enables the conversion between photovoltage and photocurrent (and *vice versa*). The bandpass behavior of the photoreceptor causes a marked sharpening of the photovoltage transient generated in response to a dim flash, without modifying much its TTP relative to that of the photocurrent (Fig. 1B): on the one hand the membrane must be charged thereby delaying response initiation, on the other the inner segment conductances promote response termination. The balance between the two effects may differ depending on the species, likely explaining why, in contrast to mouse, in salamander the dim flash TTP is shorter for the photovoltage [52]. An analogous process occurs to SPRs in rod bipolar cells [33]. Here we combined this impedance model with a novel experimental approach, inspired by the whole cell patch recordings customarily made from thin fly photoreceptors [53], whereby perforated patch clamp recordings were made directly on the rod outer segment using very fine pipettes. We found that this technique drastically reduced a run-down of rod response kinetics which tends to occur in mouse during patch recordings [28,39]. In fact our dim flash TTP with patch was: (*i*) well within the range reported with other electrophysiological techniques, (*ii*) at the lower bound of those reported for mammals with patch clamp ([39] and references therein; [54]), (*iii*) matched our original estimate of unperturbed TTPs at 36 °C [28]. Furthermore, it was only ~10 ms above our independent estimate made with the loose seal approach. Taken together our data point toward an average unperturbed TTP of mouse rod dim flash responses of 140–150 ms (Ames' medium at 37 °C). It must be noted that dim flash responses include failures, SPRs and MPRs. Restricting ourselves to those responses categorized by our procedure as SPRs, leads to a somewhat higher TTP estimate of 183 ms. In fact, we found that responses categorized as MPRs have a faster kinetics than SPRs. While this may, in part, depend upon a selection bias of our categorization algorithm, we found that even in our simulations MPRs were somewhat faster than SPRs.

Our simulations qualitatively reproduced the experimental data for the bright light stimulus paradigm, as brighter backgrounds lead to a faster response decay for the flashes. Again, we did not tune the model's parameters specifically to match the experimental responses. Quantitatively however, the simulations take longer to shut off. There are a few possible reasons for this discrepancy. A possible explanation could be that mechanisms crucial for light adaptation are missing in the DM. For example, those could be the action of calmodulin on the channels, or the long-term migration of species such as arrestin between the outer and inner segment, or more likely, the already mentioned quite speculative modeling of the rhodopsin phosphorylation dependence of kinase and arrestin binding to rhodopsin. Alternatively, the difference could also stem from the fact that we are comparing photovoltage to photocurrent, because our conversion procedure is only valid for small response amplitudes. Because the rod behaves like a bandpass filter, we would expect the photocurrent to have a faster

rising phase, but a slower shut-off, bringing the experimental data closer to the simulations.

Finally, our model supports an important role of recoverin in mediating the shutoff of the cascade in conditions of light background (Fig. 10). While removing the Ca^{2+}-mediated feedback on the rhodopsin kinase did not substantially alter photoresponses in dark-adapted conditions, when simulations of saturating flashes were repeated in the presence of increasingly bright backgrounds a significant acceleration of the recovery phase was observed (Supplementary Fig. S9, right panel), which depended on the intensity of the background light, in agreement with the paradigm of light adaptation. Therefore, while our simulations of GCAP knockout rods confirm that the GCAP-mediated Ca^{2+} feedback on the guanylate cyclase activity is the only one that occurs at very dim light intensities corresponding to the SPRs [42], they also suggest that the role of recoverin in light adaptation is fully consistent with its Ca^{2+}-dependent modulation of rhodopsin kinase activity.

In conclusion, our hybrid stochastic and deterministic modelling approach recapitulates a number of recent findings on phototransduction in vertebrates both under very dim and bright conditions. The few mismatches between experimental and simulated data suggest that some critical mechanism is currently missing, or not correctly implemented in the model; nonetheless, our comprehensive approach to phototransduction modeling at its current state allows a deep investigation of specific molecular mechanisms under both physiological and disease-associated conditions.

CRediT authorship contribution statement

Charlotte Johanna Beelen: Conceptualization, Data curation, Formal analysis, Software, Methodology, Investigation, Writing - original draft. **Sabrina Asteriti:** Data curation, Formal analysis, Methodology, Investigation. **Lorenzo Cangiano:** Methodology, Investigation, Formal analysis, Supervision, Validation, Funding acquisition, Resources, Writing - review & editing. **Karl-Wilhelm Koch:** Methodology, Investigation, Formal analysis, Supervision, Validation, Funding acquisition, Resources, Writing - review & editing. **Daniele Dell'Orco:** Methodology, Investigation, Formal analysis, Supervision, Validation, Funding acquisition, Resources, Writing - review & editing.

Declaration of Competing Interest

The authors declare that they have no known competing financial interests or personal relationships that could have appeared to influence the work reported in this paper.

Acknowledgements

This work was supported by a grant from the Foundation Telethon Italy (GGP16010) to DDO and LC and grants from the Deutsche Forschungsgemeinschaft (GRK1885 and KO 948/15-1) to KWK. CB acknowledges support from the German Academic Exchange Service (DAAD) and the Deutsche Forschungsgemeinschaft (GRK 1885). The stochastic simulations were performed at the HPC Cluster CARL, located at the University of Oldenburg (Germany) and funded by the DFG through its Major Research Instrumentation Programme (INST 184/157-1 FUGG) and the Ministry of Science and Culture (MWK) of the Lower Saxony State.

Appendix A. Supplementary data

Supplementary data to this article can be found online at https://doi.org/10.1016/j.csbj.2021.06.033.

References

[1] Koch KW, Dell'Orco D. Protein and signaling networks in vertebrate photoreceptor cells. Front Mol Neurosci 2015;8:67.
[2] Pugh Jr EN, Lamb T. Phototransduction in vertebrate rods and cones: molecular mechanisms of amplification, recovery and light adaptation. In: Stavenga D, DeGrip W, Pugh EJ, editors. Handbook of Biological Physics, North Holland. p. 183–255.
[3] Yue WWS, Silverman D, Ren X, Frederiksen R, Sakai K, Yamashita T, et al. Elementary response triggered by transducin in retinal rods. Proc Natl Acad Sci U S A 2019;116:5144–53.
[4] Whited AM, Park PS. Nanodomain organization of rhodopsin in native human and murine rod outer segment disc membranes. Biochim Biophys Acta 1848;2015:26–34.
[5] Gunkel M, Schöneberg J, Alkhaldi W, Irsen S, Noe F, Kaupp UB, et al. Higher-order architecture of rhodopsin in intact photoreceptors and its implication for phototransduction kinetics. Structure 2015;23:628–38.
[6] Hayashi F, Saito N, Tanimoto Y, Okada K, Morigaki K, Seno K, et al. Raftophilic rhodopsin-clusters offer stochastic platforms for G protein signalling in retinal discs. Commun Biol 2019;2:209.
[7] Dell'Orco D, Koch KW. A dynamic scaffolding mechanism for rhodopsin and transducin interaction in vertebrate vision. Biochem J 2011;440:263–71.
[8] Fanelli F, Dell'Orco D. Rhodopsin activation follows precoupling with transducin: inferences from computational analysis. Biochemistry 2005;44:14695–700.
[9] Cangiano L, Dell'Orco D. Detecting single photons: a supramolecular matter?. FEBS Lett 2013;587:1–4.
[10] Dell'Orco D. A physiological role for the supramolecular organization of rhodopsin and transducin in rod photoreceptors. FEBS Lett 2013;587:2060–6.
[11] Kaneshige Y, Hayashi F, Morigaki K, Tanimoto Y, Yamashita H, Fujii M, et al. Affinity of rhodopsin to raft enables the aligned oligomer formation from dimers: Coarse-grained molecular dynamics simulation of disk membranes. PLoS ONE 2020;15:e0226123.
[12] Schöneberg J, Heck M, Hofmann KP, Noe F. Explicit spatiotemporal simulation of receptor-G protein coupling in rod cell disk membranes. Biophys J 2014;107:1042–53.
[13] Dell'Orco D, Koch KW. Transient complexes between dark rhodopsin and transducin: circumstantial evidence or physiological necessity?. Biophys J 2015;108:775–7.
[14] Schöneberg J, Hofmann KP, Heck M, Noe F. Response to comment "Transient complexes between dark rhodopsin and transducin: circumstantial evidence or physiological necessity?" by D. Dell'Orco and K.-W. Koch. Biophys J 2015;108:778–9.
[15] Qureshi BM, Behrmann E, Schöneberg J, Loerke J, Burger J, Mielke T, et al. It takes two transducins to activate the cGMP-phosphodiesterase 6 in retinal rods. Open Biol 2018;8:180075.
[16] Lamb TD, Heck M, Kraft TW. Implications of dimeric activation of PDE6 for rod phototransduction. Open Biol 2018;8:180076.
[17] Hamer RD, Nicholas SC, Tranchina D, Liebman PA, Lamb TD. Multiple steps of phosphorylation of activated rhodopsin can account for the reproducibility of vertebrate rod single-photon responses. J Gen Physiol 2003;122:419–44.
[18] Hamer RD, Nicholas SC, Tranchina D, Lamb TD, Jarvinen JL. Toward a unified model of vertebrate rod phototransduction. Vis Neurosci 2005;22:417–36.
[19] Dell'Orco D, Schmidt H, Mariani S, Fanelli F. Network-level analysis of light adaptation in rod cells under normal and altered conditions. Mol Biosyst 2009;5:1232–46.
[20] Invergo BM, Montanucci L, Koch KW, Bertranpetit J, Dell'Orco D. Exploring the rate-limiting steps in visual phototransduction recovery by bottom-up kinetic modeling. Cell Commun Signal 2013;11:36.
[21] Invergo BM, Dell'Orco D, Montanucci L, Koch KW, Bertranpetit J. A comprehensive model of the phototransduction cascade in mouse rod cells. Mol Biosyst 2014;10:1481–9.
[22] Tikidji-Hamburyan A, Reinhard K, Storchi R, Dietter J, Seitter H, Davis KE, et al. Rods progressively escape saturation to drive visual responses in daylight conditions. Nat Commun 2017;8:1813.
[23] Yoshimatsu T, Schröder C, Nevala NE, Berens P, Baden T. Fovea-like photoreceptor specializations underlie single UV cone driven prey-capture behavior in zebrafish. Neuron 107 2020:320–337 e326.
[24] Dell'Orco D, Koch KW. Systems biochemistry approaches to vertebrate phototransduction: towards a molecular understanding of disease. Biochem Soc Trans 2010;38:1275–80.
[25] Ullah M, Wolkenhauer O. Stochastic approaches in systems biology. Wiley Interdiscip Rev Syst Biol Med 2010;2:385–97.
[26] Ullah M, Schmidt H, Cho KH, Wolkenhauer O. Deterministic modelling and stochastic simulation of biochemical pathways using MATLAB. Syst Biol (Stevenage) 2006;153:53–60.
[27] Lamb TD, Kraft TW. A quantitative account of mammalian rod phototransduction with PDE6 dimeric activation: responses to bright flashes. Open Biol 2020;10:190241.
[28] Cangiano L, Asteriti S, Cervetto L, Gargini C. The photovoltage of rods and cones in the dark-adapted mouse retina. J Physiol 2012;590:3841–55.
[29] Asteriti S, Cangiano L. Versatile bipolar temperature controller for custom in vitro applications. HardwareX 2020;8:e00155.

[30] Asteriti S, Dal Cortivo G, Pontelli V, Cangiano L, Buffelli M, Dell'Orco D. Effective delivery of recombinant proteins to rod photoreceptors via lipid nanovesicles. Biochem Biophys Res Commun 2015;461:665–70.
[31] Asteriti S, Gargini C, Cangiano L. Mouse rods signal through gap junctions with cones. Elife 2014;3:e01386.
[32] Perkins KL. Cell-attached voltage-clamp and current-clamp recording and stimulation techniques in brain slices. J Neurosci Methods 2006;154:1–18.
[33] Cangiano L, Gargini C, Della Santina L, Demontis GC, Cervetto L. High-pass filtering of input signals by the Ih current in a non-spiking neuron, the retinal rod bipolar cell. PLoS ONE 2007;2:e1327.
[34] Magistretti J, Mantegazza M, de Curtis M, Wanke E. Modalities of distortion of physiological voltage signals by patch-clamp amplifiers: a modeling study. Biophys J 1998;74:831–42.
[35] Della Santina L, Piano I, Cangiano L, Caputo A, Ludwig A, Cervetto L, et al. Processing of retinal signals in normal and HCN deficient mice. PLoS ONE 2012;7:e29812.
[36] Fortenbach C, Peinado Allina G, Shores CM, Karlen SJ, Miller EB, Bishop H, et al. Loss of the K+ channel Kv2.1 greatly reduces outward dark current and causes ionic dysregulation and degeneration in rod photoreceptors. J Gen Physiol 2021:153.
[37] Hutcheon B, Miura RM, Puil E. Models of subthreshold membrane resonance in neocortical neurons. J Neurophysiol 1996;76:698–714.
[38] Dell'Orco D, Dal Cortivo G. Normal GCAPs partly compensate for altered cGMP signaling in retinal dystrophies associated with mutations in GUCA1A. Sci Rep 2019;9:20105.
[39] Asteriti S, Cangiano L. Slow light response kinetics in rods points towards a perturbation of the normal cellular milieu. J Physiol 2015;593:2975–6.
[40] Chen CK, Burns ME, Spencer M, Niemi GA, Chen J, Hurley JB, et al. Abnormal photoresponses and light-induced apoptosis in rods lacking rhodopsin kinase. Proc Natl Acad Sci U S A 1999;96:3718–22.
[41] Xu J, Dodd RL, Makino CL, Simon MI, Baylor DA, Chen J. Prolonged photoresponses in transgenic mouse rods lacking arrestin. Nature 1997;389:505–9.
[42] Burns ME, Mendez A, Chen J, Baylor DA. Dynamics of cyclic GMP synthesis in retinal rods. Neuron 2002;36:81–91.
[43] Mendez A, Burns ME, Roca A, Lem J, Wu LW, Simon MI, et al. Rapid and reproducible deactivation of rhodopsin requires multiple phosphorylation sites. Neuron 2000;28:153–64.
[44] Koch KW, Dell'Orco D. A calcium-relay mechanism in vertebrate phototransduction. ACS Chem Neurosci 2013;4:909–17.
[45] Marino V, Riva M, Zamboni D, Koch KW, Dell'Orco D. Bringing the Ca(2+) sensitivity of myristoylated recoverin into the physiological range. Open Biol 2021;11:200346.
[46] Heck M, Hofmann KP, Kraft TW, Lamb TD. Phototransduction gain at the G-protein, transducin, and effector protein, phosphodiesterase-6, stages in retinal rods. Proc Natl Acad Sci U S A 2019;116:8653–4.
[47] Dell'Orco D, Seeber M, Fanelli F. Monomeric dark rhodopsin holds the molecular determinants for transducin recognition: insights from computational analysis. FEBS Lett 2007;581:944–8.
[48] Fanelli F, Dell'Orco D. Dark and photoactivated rhodopsin share common binding modes to transducin. FEBS Lett 2008;582:991–6.
[49] Field GD, Rieke F. Nonlinear signal transfer from mouse rods to bipolar cells and implications for visual sensitivity. Neuron 2002;34:773–85.
[50] Ala-Laurila P, Rieke F. Coincidence detection of single-photon responses in the inner retina at the sensitivity limit of vision. Curr Biol 2014;24:2888–98.
[51] Pulvermuller A, Maretzki D, Rudnicka-Nawrot M, Smith WC, Palczewski K, Hofmann KP. Functional differences in the interaction of arrestin and its splice variant, p44, with rhodopsin. Biochemistry 1997;36:9253–60.
[52] Baylor DA, Nunn BJ. Electrical properties of the light-sensitive conductance of rods of the salamander Ambystoma tigrinum. J Physiol 1986;371:115–45.
[53] Asteriti S, Liu CH, Hardie RC. Calcium signalling in Drosophila photoreceptors measured with GCaMP6f. Cell Calcium 2017;65:40–51.
[54] Reingruber J, Ingram NT, Griffis KG, Fain GL. A kinetic analysis of mouse rod and cone photoreceptor responses. J Physiol 2020;598:3747–63.